

Machine Learning Force Fields for Defective WSe₂

**Based on the Equivariant Graph Neural Network
MACE**

BACHELOR'S THESIS

submitted in partial fulfillment of the requirements for the degree of

Bachelor of Science

in

Technical Physics

by

Sebastian Kindl

Registration Number 12202366

to the Faculty of Physics
at the TU Wien
Advisor: Prof. Florian Libisch
Assistance: Max Sinner, MSc

Vienna, October 24, 2025

Sebastian Kindl

Florian Libisch

Machine Learning Force Fields for Defective WSe₂

**Bases on the Equivariant Graph Neural Network
MACE**

BACHELORARBEIT

zur Erlangung des akademischen Grades

Bachelor of Science

im Rahmen des Studiums

Technische Physik

eingereicht von

Sebastian Kindl

Matrikelnummer 12202366

an der Fakultät für Physik
der Technischen Universität Wien
Betreuung: Prof. Florian Libisch
Mitwirkung: Max Sinner, MSc

Wien, 24. Oktober 2025

Sebastian Kindl

Florian Libisch

Declaration of Authorship

Sebastian Kindl

I hereby declare that I have written this Bachelor's Thesis independently, that I have completely specified the utilized sources and resources and that I have definitely marked all parts of the work - including tables, maps and figures - which belong to other works or to the internet, literally or extracted, by referencing the source as borrowed.

I further declare that I have used generative AI tools only as an aid, and that my own intellectual and creative efforts predominate in this work. In the appendix "Overview of Generative AI Tools Used" I have listed all generative AI tools that were used in the creation of this work, and indicated where in the work they were used. If whole passages of text were used without substantial changes, I have indicated the input (prompts) I formulated and the IT application used with its product name and version number/date.

Vienna, October 24, 2025

Sebastian Kindl

Acknowledgements

I would like to express my sincere gratitude to my supervisors, Florian Libisch and Max Sinner, for their invaluable support and trustful collaboration throughout the course of this thesis.

Kurzfassung

Defekte in zweidimensionalen Halbleitern wie Wolframdiselenid führen zur Ausbildung von Einzelphotonenquellen und bilden damit ein Fundament für viele quantenphotonische Anwendungen. Als mikroskopischer Ursprung dieses Phänomens wird das Zusammenspiel zwischen Defekten in der atomaren Struktur und lokalen Dehnungen postuliert, welches die Bildung von lokalisierten Exzitonen innerhalb der Bandlücke begünstigt. In dieser Arbeit wird ein Ansatz vorgestellt, der das äquivariante Graph-Neural-Network MACE auf atomaren Konfigurationen trainiert, welche aus DFT-Berechnungen hervorgehen. Dieses Modell ist in der Lage, interatomare Wechselwirkungen zu erlernen und dabei bedeutsame Symmetrien, wie die Rotationsäquivarianz, zu berücksichtigen. Das Ziel ist die Untersuchung von Defektgeometrien, welche zur Bildung von Intervalley-Defektexzitonen führen, welche wiederum als mikroskopischer Ausgangspunkt einzeln emittierter Photonen gelten. Die vorgestellte Methode bietet damit eine effiziente und skalierbare Möglichkeit zur Untersuchung komplexer Phänomene, die durch Defekte in zweidimensionalen Materialien verursacht werden.

Abstract

Single-photon emitters in two-dimensional semiconductors, such as tungsten diselenide, have emerged as promising candidates for quantum photonic applications. The microscopic origin of this effect is connected to the interplay between local strain modulations and point defects, which result in defect states within the band gap localized at the defect site, resulting in strongly localized so-called Frenkel excitons . In this thesis, the formation and characteristics of such single-photon emitters are studied using state-of-the-art machine learning force fields. In particular, the equivariant graph neural network MACE is trained on a defective structure produced by DFT calculations. This model is capable of learning interatomic interactions while preserving key symmetries, such as rotational equivariance. The MACE model is applied on strained defect configurations with the aim to capture the formation of intervalley defect excitons proposed as the microscopic origin of single emitted photons. The presented methods provide a fast and scalable way to investigate quantum phenomena caused by defects in two-dimensional materials.

Contents

Kurzfassung	ix
Abstract	xi
Contents	xiii
1 Introduction	1
1.1 Structure of the Thesis	2
2 Theoretical Background	3
2.1 Two-Dimensional Materials and tungsten diselenide (WSe_2)	3
2.2 Phonons and Lattice Vibrations	4
2.3 Defects and Single-Photon Emitters in WSe_2	7
2.4 Machine Learning Force Fields	8
2.5 Message Passing Graph Neural Networks for Atomistic Modeling	9
2.6 MACE: An Equivariant Message Passing Neural Network Model	10
3 Methods and Implementation	13
3.1 Overview and Objectives	14
3.2 Dataset Generation and Preprocessing	14
3.3 Computational Workflow	17
3.4 Model Training and Hyperparameters	18
3.5 Model Evaluation and Validation	20
4 Results and Discussion	21
4.1 Phonon Properties of Pristine WSe_2	22
4.2 Phonon Properties of Defective WSe_2	23
4.3 Comparative Analysis: Pristine vs Defect	24
4.4 Localized Vibrational Modes around the Vacancy	25
4.5 Physical Interpretation and Limitations	26
4.6 Summary of Results	27
5 Conclusion and Outlook	29
5.1 Conclusion	29

5.2 Outlook	29
Overview of Generative AI Tools Used	31
List of Figures	33
Acronyms	37
Bibliography	39

CHAPTER

1

Introduction

Two-dimensional materials, especially the transition metal dichalcogenides (TMDCs), have attracted attention in modern materials science by bringing new possibilities due to their unique electronic and optical properties. Among this class of materials, monolayer WSe₂ is subject of ongoing research due to its unique physical properties like a direct band gap, strong spin-orbit coupling, valley-selective excitonic transitions, and the resulting plethora of potential applications in optoelectronics and photonics.

A phenomenon of particular interest observed in WSe₂ is the emission of single photons. These single-photon emitter (SPE) are believed to originate from defect excitons and local strain-fields. Due to the complexity of defect-induced lattice deformations and the resulting changes in the electronic structure, understanding the underlying physics and predicting the formation of such localized states remains a challenge.

Density Functional Theory (DFT) simulations offer accurate insight into such systems, but are computationally expensive and time-consuming when large or defective systems are involved. The development of machine-learned interatomic potentials based on a Graph Neural Network (GNN) have helped to overcome these limitations, as they allow efficient approximations with near-DFT accuracy while also reducing the computational cost.

In this thesis, an equivariant architecture of a GNN, the MACE model, is trained on DFT data to provide machine-learned force fields for defective WSe₂ structures. This model considers symmetries such as rotation and permutation equivariance, which is essential for accurate predictions in atomistic simulations and is applied to defect configurations in monolayer WSe₂ with the aim of efficiently model defect-induced quantum phenomena.

1.1 Structure of the Thesis

This thesis is structured as follows:

Ch. 2 will provide an introduction to the theoretical background needed for this thesis. We will begin with basics of solid-state physics involving two-dimensional materials, phonons, defects, and the resulting emission of single photons. This will be followed by an introduction to machine learning force fields and key properties of the model used in this thesis.

Ch. 3 will introduce the implementation and present the training of the neural network. A discussion of relevant parameters and training conditions followed by an evaluation of the MACE model will also be shown.

Ch. 4 will present the results and a discussion. The chapter opens with the phonon properties of pristine tungsten diselenide and then moves on to defective systems containing a selenium vacancy. A comparative analysis across different supercell sizes highlights defect-induced features and localized vibrational modes around the defect. This chapter concludes with a short interpretation of the findings and a brief discussion.

Ch. 5 provides the overall conclusion and an outlook for the future. It summarizes the main results and findings produced with the MACE model and provides insight into future applications and directions of work.

CHAPTER 2

Theoretical Background

This chapter introduces the theoretical foundations necessary to understand the ideas and methods applied in this thesis. After presenting two-dimensional materials with a focus on monolayer WSe₂, the consequences of atomic defects and their connection to single-photon emission are discussed. Furthermore, the approach of using machine learning methods in atomistic simulations is demonstrated, with a focus on GNNs for modeling atomic interactions. Finally, the architectures of the MACE model, as well as the relevance of its equivariant character, are presented in detail.

2.1 Two-Dimensional Materials and WSe₂

Two-dimensional materials are solids consisting of a single layer of atoms. Their reduced dimensionality results in unique optical and electronic properties which are not seen in their bulk counterparts.

Among the class of 2D materials are the so-called TMDCs, which consist of a transition metal (M) such as tungsten or molybdenum, and a chalcogen (X) such as sulfur or selenium in the form of MX_2 . Monolayer versions of these materials represent semiconductors with a direct band gap, which makes them useful in different optoelectronic applications [1].

The material of interest in this thesis is tungsten diselenide WSe₂, a transition metal dichalcogenide (TMDC). It offers a direct bandgap and – due to the reduced dimensionality – the dielectric screening is much weaker than in three-dimensional materials. As a result, these materials feature a much larger exciton binding energy, i.e., the binding energy between an electron in the conduction band and a hole in the valence band. Excitons are thus more stable and more tightly bound than in 3D bulk materials [2].

Moreover, the strong spin-orbit interaction results in well-separated valence and conduction bands at the K and K' areas of the Brillouin zone. Due to spin-valley locking, each of

2. THEORETICAL BACKGROUND

those valleys correlates with a certain spin orientation (i.e., opposite signs of the spin-orbit splitting for the two valleys). Optical selection rules thus allow circular polarized light to selectively excite a single valley - allowing valley-specific optical excitation [2].

Since the sign of the spin-orbit splitting for the conduction and valence bands is identical for WSe₂, the lower-lying conduction band state has the opposite spin of the higher-lying valence band. Consequently, optical de-excitation is spin-forbidden. Defect sites, however, allow to bypass momentum conservation, and thus for optical de-excitation via the other valley. As a consequence, one finds localized SPEs caused by excitons trapped at atomic defects. As the band gap decreases with strain, local strain fields funnel these excitons towards defects where they become trapped, enabling optical transitions [3].

This mechanism also allows the formation of localized intervalley defect excitons, where the electron and its correlated hole are located in opposite valleys. Transitions between opposite valleys are formally forbidden. However, defects in the structure break momentum conservation, and thus the valley-symmetry, allowing the recombination of excitons resulting in the emission of single photons [3].

2.2 Phonons and Lattice Vibrations

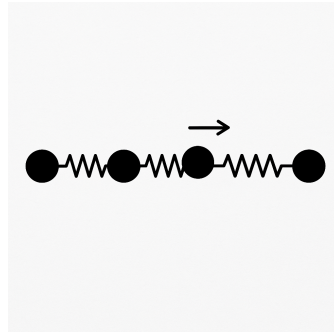


Figure 2.1: Schematic illustration of a monoatomic linear chain with a longitudinal displacement of a single atom [4]

According to [5] and [6], many physical properties of solid bodies – such as thermal and electronic transport – rely on the motion of atoms in a crystal lattice. In quantum physics, the quantization of these motions or vibrations are represented by quasi-particles called phonons.

2.2.1 Fundamentals and Phonon Dispersion Relation

Rather than remaining still, the atoms in a crystal lattice oscillate around their equilibrium positions. These vibrations are the result of the restoring forces of the atom and can, within the harmonic approximation, be described as coupled harmonic oscillators with well-defined wave vector q and frequency ω [5]. In principle, one distinguishes two different

types of phonons: acoustic and optical phonons. Acoustic phonons describe the in-phase movement of atoms which corresponds to sound waves, while optical phonons describe the out-of-phase movement [6].

The dispersion relation $\omega(q)$ shows the relation between the vibrational frequency ω and the wave vector q , providing information on how the phonons propagate in the crystal lattice, which in turn determines different properties, such as the phonon density of states, which will be shown in the next section [5]. Each solution of the dynamical equations corresponds to a branch of this dispersion relation, which can be illustrated as curves in reciprocal space or k -space, as will be shown for the diatomic chain.

In general, for a crystal consisting of N atoms there exist $3N$ branches, while the factor three shows the number of dimensions or degrees of freedom. Regardless of the number of atoms, three of these branches are always acoustic while the remaining $3N - 3$ branches are optical [5], [6].

One-Dimensional Monoatomic Chain

To better understand the concepts discussed below, we introduce the simplest model of a solid - the one-dimensional monoatomic linear chain. Here, all atoms are identical with mass m , and connected by springs with spring constant K . Since only small deflections are considered, the restoring force can be described using Hooke's law.

One-Dimensional Diatomic Chain

The one-dimensional diatomic linear chain represents the extension of the monoatomic chain. As the name suggests, the diatomic chain is characterized by two atoms in its unit cell which allows for two degrees of freedom per wave vector and hence two distinct phonon branches. The acoustic branch is the same as in the monoatomic case, while the additional optical branch is directly caused by the increased number of atoms in the unit cell what leads to an increased number of vibrational degrees of freedom.

2.2.2 Phonon Density of States

The phonon Density of States (DOS) $g(\omega)$ provides the number of vibrational modes per frequency interval and is used for different thermodynamic calculations as well as understanding phonon-induced interactions. It provides a direct connection to the phonon dispersion relation by counting available q -states corresponding to a specific frequency interval. Formally it can be written as:

$$g(\omega) \propto \left| \frac{dq}{d\omega} \right| \quad (2.1)$$

which suggests a correlation between the DOS and the dispersion relation.

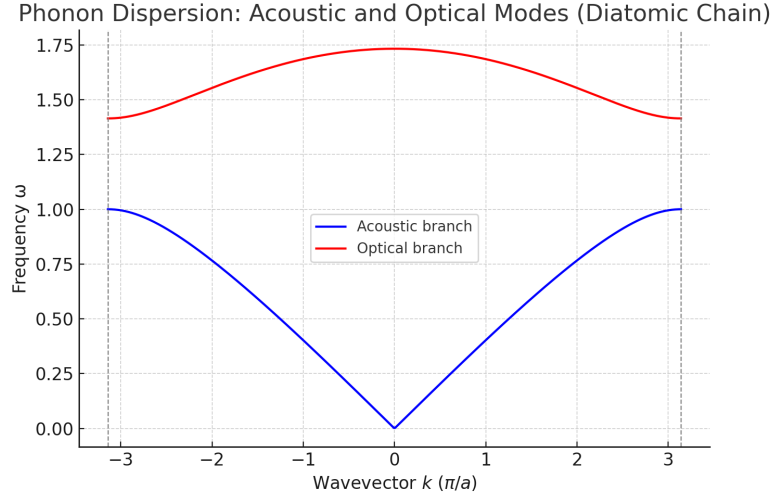


Figure 2.2: Dispersion of Diatomic Chain: Acoustic and Optical Modes, calculated using ASE.

Within the Debye model, the phonon DOS varies with dimensionality. In one dimension $g(\omega)$ stays constant, in two dimensions, it scales as $g(\omega) \propto \omega^2$ and in three dimensions as $g(\omega) \propto \omega^3$, showing the strong influence of dimensionality on vibrational phonon properties.

2.2.3 Phonons in Two-Dimensional Materials

As already discussed in 2.2.2, phonon properties strongly depend on the dimensions of the system. Reduced dimensionality therefore changes the phonon dispersion as well as the DOS, which in turn affects other material properties such as thermal transport [5]. In monolayer WSe₂, the electron-phonon interaction becomes stronger due to weaker dielectric screening, leading to tightly bound excitons [2]. Further, the interaction between phonons, atomic defects, and local strain fields leads to a modified electronic structure, which in turn results in localized excitonic states.

2.2.4 Phonon-Defect Interactions

Ideal crystals provide a certain translational periodicity throughout the entire lattice. Defects, regardless of their type, break this symmetry and act as scatter centers for phonons that would normally propagate freely through the lattice. In kinetic theory, the thermal conductivity provides insight into how efficiently heat is conducted through the material and an expression can be found as:

$$\kappa \sim \frac{1}{3} C v^2 \tau \quad (2.2)$$

where C is the specific heat, v the average group velocity of the phonons and τ their relaxation time. As defects cause phonons to scatter, their velocity and relaxation time decrease, leading to a weaker thermal conductivity.

2.3 Defects and Single-Photon Emitters in WSe₂

In monolayer WSe₂, the strong spin-orbit coupling is a consequence of the heavy atomic masses of tungsten (W) and selenium (Se) and affects the electronic structure. Especially in the K and K' valleys of the Brillouin Zone (BZ), the strong spin-orbit coupling lifts the spin degeneracy of the valence band by a few hundred meV, which results in spin-polarized electronic states with opposite orientations. The separation of these valleys provides the basis for *valleytronics* [3], which describes valley-selective optical excitation using circularly polarized light. Excitons – electron-hole pairs – strongly affect optical properties in WSe₂.

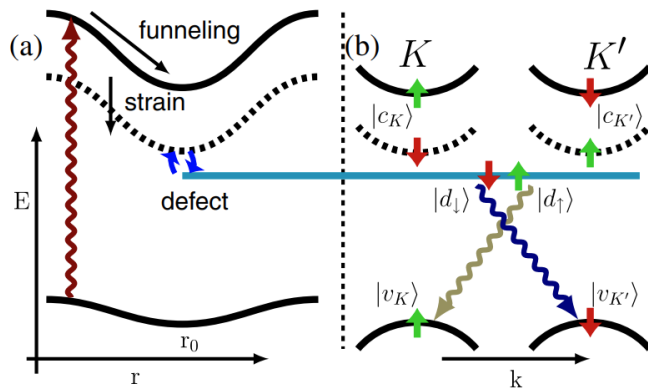


Figure 2.3: Schematic illustration of single-photon emitter in WSe₂, taken from [3].

Depending on the various spin and valley configurations, two different types of excitons can emerge: *bright* and *dark* excitons. Defects in the crystal lattice influence the electronic and vibrational structure by breaking the symmetry of the lattice, introducing localized electronic states within the band gap that can trap excitons. The recombination of excitons is followed by the emission of a single photon - the single-photon emitter. In addition, local strain fields can further influence the electronic band structure, thereby enhancing localized excitonic states. The combination of defects with these local strain fields can result in an electron and a hole in opposite valleys, called *intervalley defect excitons*. While transitions between those valleys are forbidden in pristine configurations, the broken symmetry of defective structures enables the recombination of these intervalley excitons, which are proposed as the microscopic origin of single-photon emission in monolayer WSe₂.

2.4 Machine Learning Force Fields

In computational materials science, force fields are used to describe the interaction between atoms or molecules. While traditional force fields are built on simple equations and different parameters with a very limited flexibility and accuracy, Machine Learning Force Field (MLFF)s provide a promising alternative [7].

Machine-learning-based force fields are models that predict forces and potential energies of atomic configurations by learning the underlying physics of these structures directly from reference data, typically generated through DFT calculations with high computational cost. Once a model is trained, it can predict the forces and energies of new structures with near-DFT accuracy, but in significantly less time [7]. Traditional force fields work well for simple structures, but they often fail when applied to more complex structures such as materials with defects, and that is where MLFFs come to play [7].

MLFFs can be described as a supervised regression problem [8]. A model h_θ with trainable parameters θ connects a specific input configuration x , such atomic positions and atomic species, to predictions y_{pred} , such as total energies E or atomic forces \mathbf{F} :

$$y_{\text{pred}} = h_\theta(x). \quad (2.3)$$

The aim is to minimize a loss function \mathcal{L} that describes the difference between predicted values y_{pred} and some reference data y_{true} obtained from DFT calculations:

$$\mathcal{L}(\theta) = \frac{1}{N} \sum_{i=1}^N \|y_{\text{pred}}^{(i)} - y_{\text{true}}^{(i)}\|^2. \quad (2.4)$$

The loss function \mathcal{L} can also be written using energies and forces:

$$L(\theta) = w_E \|E_{\text{pred}} - E_{\text{true}}\|^2 + w_F \|\mathbf{F}_{\text{pred}} - \mathbf{F}_{\text{true}}\|^2. \quad (2.5)$$

Overall, the goal is to determine the parameters that minimize this loss:

$$\theta^* = \arg \min_{\theta} L(\theta). \quad (2.6)$$

The concept of MLFFs is to train a model on atomic structures provided by DFT calculations. These datasets are each labeled with atomic forces and total energy allowing the model to learn the correlation between energy, forces and the relative positions of atoms [7].

2.5 Message Passing Graph Neural Networks for Atomistic Modeling

GNNs are a class of neural networks developed for graph-structured data and have become a central tool in materials science for modeling atomistic systems due to their ability to capture the underlying physics [9]. While classic neural networks operate on vectors or images, GNNs not only consider the entities itself but also their relationships such as forces between single atoms.

Graphs are mathematical objects consisting of nodes and edges and are used to capture relationships in data. In the context of modeling atomistic systems, nodes represent the atoms and edges the interaction between these atoms providing a natural and flexible way for describing such systems [9].

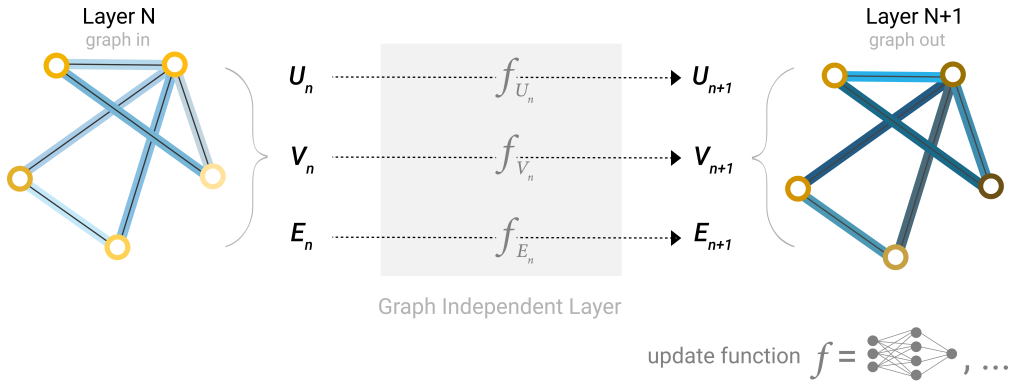


Figure 2.4: Schematic illustration of a single GNN layer, taken from [10]. Every node, edge and global feature vector are updated by separate MLPs, while the graph connectivity stays fixed

Message Passing Neural Network (MPNN)s for modeling atomic systems represent a subclass of GNNs, as introduced by Gilmer et al. [9]. The process behind these MPNNs consists of two essential steps: message passing and readout. In the message passing phase, the atomic features are iteratively updated by aggregating information from neighbor atoms. After the message passing phase is complete, a readout function produces graph-structured predictions.

MPNNs are specifically used for modeling atomistic systems due to their ability to consider key properties such as permutation or translation invariance, but also show a notable limitation: they do not consider rotational or reflection symmetries, leading to poor generalization. To overcome this limitation, the MPNN framework is extended with an equivariant approach [11].

2.6 MACE: An Equivariant Message Passing Neural Network Model

In atomic systems, fundamental laws and underlying symmetries need to be considered to make correct predictions. While traditional neural network architectures often ignore those aspects, certain equivariant models are designed to respect symmetries like translation, rotation, or permutation invariance [12].

The MACE model represents a state-of-the-art equivariant graph neural network aiming to model highly accurate force fields on many-body interactions and rotational equivariance, as introduced by Batatia et al. [11]. All concepts and architectural components described in the following sections are based on their work.

2.6.1 Concept

The idea behind the MACE model is a message passing neural network that respects physical key symmetries, especially the equivariance under the SO(3) group which includes rotation, translation, as well as reflection. This approach is essential for modeling real atomic structures so that the predicted forces and energies transform consistently with the configuration of the atomistic structure. The model is built on a regular MPNN framework, but is improved by implementing certain symmetry-respecting tools. On the one hand, it uses the spherical harmonics to respect directional information. On the other hand, it uses parts of the SO(3) group, which describes all possible rotations in three-dimensional space. The atomic features are no longer considered as scalars, but as equivariant features in the form of tensors that transform under rotation. Furthermore, the concept of multipole aggregation is implemented, with the aim of better describing many-body interactions by processing information about neighboring atoms in a way that respects symmetries of the system.

2.6.2 Architecture

MACE is built upon the usual MPNN framework, but also brings in the following innovations to improve accuracy and performance.

As introduced by Batatia et al. [11], in each message passing iteration t , the message $m_i^{(t)}$ for atom i is constructed as a sum over many-body interactions in the order of $\nu + 1$:

$$\mathbf{m}_i^{(t)} = \sum_j \mathbf{u}_1(\boldsymbol{\sigma}_i^{(t)}; \boldsymbol{\sigma}_j^{(t)}) + \sum_{j_1, j_2} \mathbf{u}_2(\boldsymbol{\sigma}_i^{(t)}; \boldsymbol{\sigma}_{j_1}^{(t)}, \boldsymbol{\sigma}_{j_2}^{(t)}) + \dots + \sum_{j_1, \dots, j_\nu} \mathbf{u}_\nu(\boldsymbol{\sigma}_i^{(t)}; \boldsymbol{\sigma}_{j_1}^{(t)}, \dots, \boldsymbol{\sigma}_{j_\nu}^{(t)}) \quad (2.7)$$

Here $\boldsymbol{\sigma}_i^{(t)}$ is the state of atom i in the layer t and each u_k represents a learnable function that contains correlations between atom i and its neighbors.

Message Construction

The message construction begins by calculating the basis coefficients $A^{(t)}$ containing directional information with the Clebsch-Gordan coefficients C and spherical harmonics Y_l^m .

$$A_{i,kl_3m_3}^{(t)} = \sum_{l_1m_1,l_2m_2} C_{l_1m_1,l_2m_2}^{l_3m_3} \sum_{j \in \mathcal{N}(i)} R_{kl_1l_2l_3}^{(t)}(r_{ji}) Y_{l_1}^{m_1}(\hat{\mathbf{r}}_{ji}) \sum_{\tilde{k}} W_{k\tilde{k}l_2}^{(t)} h_{j,\tilde{k}l_2m_2}^{(t)} \quad (2.8)$$

$$A_{i,kl_1m_1}^{(1)} = \sum_{j \in \mathcal{N}(i)} R_{kl_1}^{(1)}(r_{ji}) Y_{l_1}^{m_1}(\hat{\mathbf{r}}_{ji}) W_{kz_j}^{(1)} \quad (2.9)$$

The resulting coefficients are used to compute higher-order tensor products $B^{(t)}$, providing a message basis that respects rotational symmetries.

$$B_{i,\eta_\nu kLM}^{(t)} = \sum_{lm} C_{\eta_\nu,lm}^{LM} \prod_{\xi=1}^{\nu} \sum_{\tilde{k}} w_{\tilde{k}k\ell_\xi}^{(t)} A_{i,\tilde{k}\ell_\xi m_\xi}^{(t)}, \quad lm = (l_1m_1, \dots, l_\nu m_\nu) \quad (2.10)$$

The final message $m_i^{(t)}$ is ultimately computed by the sum of all $B^{(t)}$ components by using learnable functions as weights.

$$m_{i,kLM}^{(t)} = \sum_{\nu} \sum_{\eta_\nu} W_{z_ikL,\eta_\nu}^{(t)} B_{i,\eta_\nu kLM}^{(t)} \quad (2.11)$$

Update

The atomic feature $\sigma_i^{(t)}$ is updated in each layer by comparing the current state of the atom i with a neighbor message $m_i^{(t)}$ using an update function U_t .

$$h_{i,kLM}^{(t+1)} = U_t^{kL} (\boldsymbol{\sigma}_i^{(t)}, \mathbf{m}_i^{(t)}) = \sum_{\tilde{k}} W_{kL,\tilde{k}}^{(t)} m_{i,\tilde{k}LM}^{(t)} + \sum_{\tilde{k}} W_{z_ikL,\tilde{k}}^{(t)} h_{i,\tilde{k}LM}^{(t)} \quad (2.12)$$

Readout

After multiple message passing layers, the total energy of the system E_i can be obtained by summing over all energy contributions $E_i^{(t)}$. For layers $t < T$, the correlation of the atomistic features and the single energy contributions $E_i^{(t)}$ is linear using learnable weights. For the final layer T , a multi-layer perceptron (MLP) is used.

$$E_i = E_i^{(0)} + E_i^{(1)} + \cdots + E_i^{(T)}, \quad \text{where}$$
$$E_i^{(t)} = \mathcal{R}_t \left(h_i^{(t)} \right) = \begin{cases} \sum_{\tilde{k}} W_{\text{readout}, \tilde{k}}^{(t)} h_{i, \tilde{k}00}^{(t)} & \text{if } t < T \\ \text{MLP}_{\text{readout}}^{(t)} \left(\left\{ h_{i, k00}^{(t)} \right\}_k \right) & \text{if } t = T \end{cases} \quad (2.13)$$

2.6.3 Application in This Work

In this work, the MACE model is used to accurately approximate interatomic forces and energies of a WSe₂ structure. The model is trained on defect-induced monolayer WSe₂ obtained by DFT calculations with the goal of investigating the influence of the defect on optical and electronic structures. The dataset used for training consists of relative atomic positions, total energies, and forces in the form of vectors. Once the model is trained correctly and has captured certain correlations in the defected structure, it can predict forces and energies for new atomic configurations with high accuracy. These predictions enable other calculations such as relaxing atomic structures or computing phonon spectra while also considering all relevant symmetries.

CHAPTER

3

Methods and Implementation

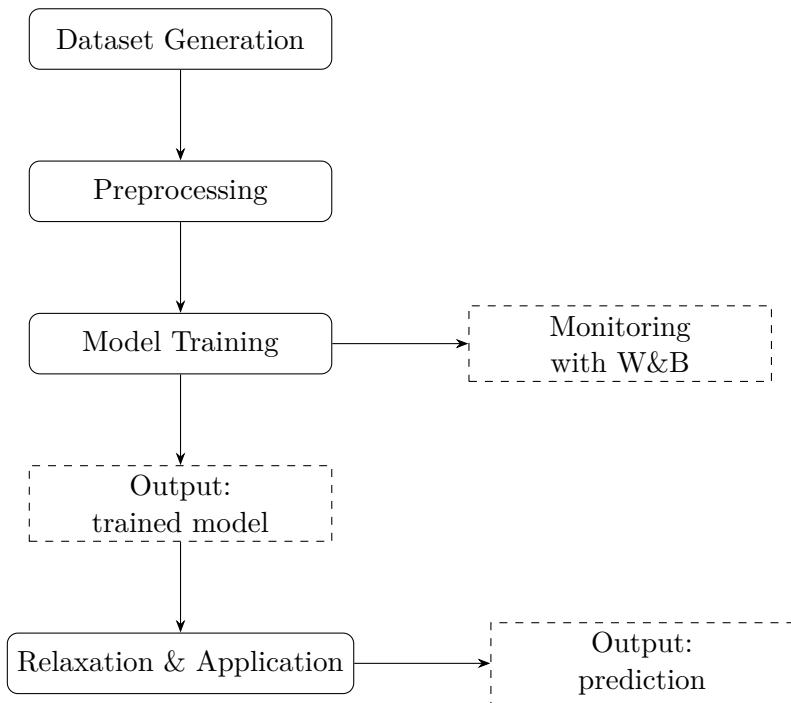


Figure 3.1: Pipeline of the project: from DFT data generation to training, evaluation, and application of the trained MACE model.

This chapter presents the methods used to analyze defect-induced monolayer WSe₂ using MLFFs. After a brief overview of the situation, the generation of datasets is explained. In addition, the actual training of the MACE model as well as the evaluation strategies

3. METHODS AND IMPLEMENTATION

are described. Finally, an application of the trained model to defective structures is presented, in order to investigate the effect of the single-photon emitter.

The following sections contain:

- Dataset generation
- Model training and evaluation
- Application to defect structures

3.1 Overview and Objectives

The primary goal of this thesis is to apply machine-learned interatomic potentials to model defective monolayer WSe₂. In order to accurately model real atomistic systems, an equivariant approach of a graph neural network is used - the MACE model. To train the model, structural data obtained by DFT calculations is used, which are provided in a .xyz file. This file contains interatomic forces, total energies, and relative atomic positions, whose correlations can be learned by the MACE model.

The training itself is carried out on a GPU to accelerate the optimization process and is monitored through the Weights & Biases (W&B) interface, enabling a real-time tracking of essential metrics. Once the training is done, the model is capable of approximating forces and energies of new structures.

The trained model enables calculations of energies and forces of different structures with near-DFT accuracy and the relaxation of structures with reduced computational cost. In addition, it is capable of performing calculations of the dispersion relation as well as DOS for both relaxed and pristine systems, allowing a direct comparison.

3.2 Dataset Generation and Preprocessing

Before the actual training of the MACE model, it is essential to understand how the training data was generated. To create accurate MLFFs, representative datasets of atomic configurations are needed, which leads to expensive DFT calculations. The high computational cost of these calculations can be reduced by using different approaches. First, the acceleration of ab-initio DFT calculations using the MLFF extension in VASP is shown. Next, the implementation of active learning, which selectively adds only the most informative configurations, and its impact on the efficiency of dataset generation are discussed. Finally, the resulting dataset, its structure, and its implementation in MACE are described.

VASP Machine Learning Force Fields

The Vienna Ab-initio Simulation Package (VASP) is one of the most widely used tools for structural DFT calculations. The implementation of MLFFs into VASP enables

calculations without a significant decrease in accuracy while, at the same time, drastically lowers the computational cost. Instead of solving the Kohn-Sham equations, which normally form the basis of typical DFT calculations, the implemented MLFFs use descriptors for the prediction of atomic energies and forces. These descriptors capture information about the atomic structure, such as atomic distances and angles, while also preserving the symmetry of the system. After calculating the energies and forces for both pristine and defective configurations using DFT, the MLFF extension learns the underlying potential energy surface (PES), which allows the prediction of new defect configurations [7].

Active Learning

Active Learning, in particular on-the-fly training, is another tool to reduce the computational cost of DFT calculations for structural simulations. Instead of calculating a large number of structures to create a diverse dataset, this approach only adds those configurations to the dataset that include the most information. When the model encounters a configuration that strongly deviates from its usual training data, the predictive variance increases, acting as an indicator for additional DFT calculations for that specific configuration. The new data are added to the training set and enable the improvement of the model while needing less expensive DFT queries. This means that the Kohn-Sham equations only need to be solved in regions of uncertainty. Hence, instead of evaluating the structure of all sampled geometries, DFT calculations are restricted to the most informative regions.

It is useful to compare this process to Bayesian optimization since both methods estimate uncertainties. While Bayesian optimization intentionally selects new points in areas with high variance that might maximize a certain acquisition function, active learning, in contrast, minimizes the overall variance across the domain, which can therefore be expressed as an *arg min* problem:

$$\min \mathbb{E}_{p(x)} [\ell(f^*(x), f(x))]. \quad (3.1)$$

This strategy ensures data efficiency, leading to a faster convergence of the model.

3. METHODS AND IMPLEMENTATION

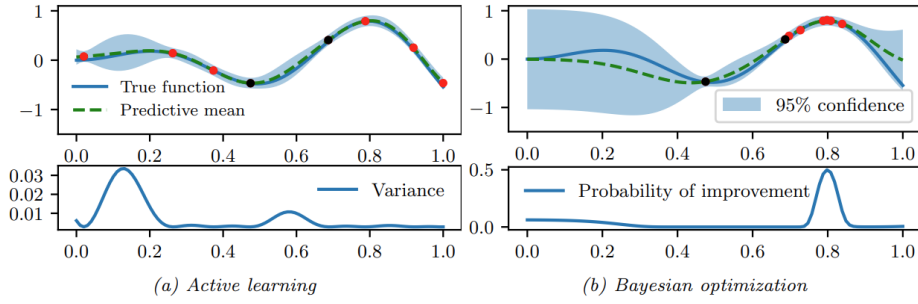


Figure 3.2: Comparison of active learning (a) and Bayesian optimization (b), taken from [13].

As shown in Figure 3.2, active learning iteratively improves its predictive mean to approximate the actual function, while Bayesian optimization focuses on regions with the highest probability of improvement.

Dataset

The dataset used to train the MACE model was obtained from DFT calculations of monolayer WSe₂ and stored in the .xyz file format. A typical block of this dataset contains:

- Lattice vectors
- Element type and positions
- Forces of each atom
- Global properties such as the total energy and stress tensor

A shortened example of the dataset in .xyz format is shown below:

```

3
Lattice="3.3064 0.0000 -0.0000 -1.6532 2.8634 0.0000
-0.0000 0.0000 13.0779" Properties=species:S:1:pos:R:3:forces:R:3
energy=-22.6457 pbc="T T T"
W 1.6532 0.9545 9.8084 -0.00005 -0.00023 0.00003
Se -0.0000 1.9090 8.1163 0.00008 0.00007 0.3126
Se -0.0000 1.9090 11.5006 -0.00000 0.00016 -0.3126

```

Here, the first line shows the number of atoms in this configuration while the second line provides cell parameters and global properties. The last three lines provide the elements together with their relative positions and their atomic force components.

3.3 Computational Workflow

3.3.1 Overview

The following computational workflow provides insight into the internal processes, from the actual training to the various results.

The reference data are used for the training process, in which the MACE model constructs MLFFs by learning the underlying PES of the structure. Once the training is complete, a `.model` file is provided, enabling atomic simulations using Atomic Simulation Environment (ASE) and vibrational analysis using Phonopy.

The usual pipeline can be divided into the following steps:

1. Integration of Reference Data
2. Model Training
3. Evaluation and Structural Relaxation
4. Defect Implementation, Vibrational Analysis and Comparison

3.3.2 MLFF Construction (MACE Framework)

This section is an extension of the information provided in 2.6. The MACE model learns the interactions between the various atoms directly from the provided reference data, where each configuration is represented by a graph. Internally, the data are stored in either NumPy or PyTorch tensors, containing atomic numbers, relative positions, and information about neighboring atoms, and enabling fast calculations on GPUs. By expanding neighbor vectors into spherical harmonics and radial basis functions, the MACE model constructs a local environment descriptor for every single atom. This introduces irreducible representations, or short , which build the core of the $E(3)$ -equivariance and ensure predictions that are translation-invariant, permutation-invariant, and rotation-equivariant. Summation over the per-atom energies obtained by the final readout yields the total energy, which enables calculations of the forces by differentiation.

3.3.3 Structural Relaxation and Force Evaluation

Once converged, the trained model is stored in a `.model` file, which provides the basis for interatomic calculations using ASE, connecting the machine-learned potential to a simulation interface. This interface is then used for energy and force evaluations.

For accurate physical predictions, structural relaxations are needed. These relaxations enable geometrical optimizations and are performed using the ASE calculator. The relaxed atomic configurations are stored in `.xyz` files, which are further used as structural reference data.

3. METHODS AND IMPLEMENTATION

Vibrational analysis and DOS calculations are performed using Phonopy. It uses the finite displacement method, which means that the atoms in the relaxed structure are displaced by only a small distance, and for each displacement the MACE model delivers the forces. Phonopy then creates the dynamical matrix, diagonalizes it, and thereby determines the eigenvalues. This procedure creates the phonon band structure and other phonon properties used for vibrational analysis.

3.3.4 Defect Construction, Supercell Expansion and Evaluation

ASE is also used for vibrational analysis of defective WSe₂. After supercells are created, defects are introduced by removing single atoms from the pristine crystal lattice, breaking the local symmetry. After the implementation of the defect, the defective structure is relaxed and compared to the pristine version to identify localized vibrational modes and shifts in the Projected Density of States (PDOS). Moreover, expansion of supercell sizes allows the distinction of finite-size effects.

3.4 Model Training and Hyperparameters

In the following, the entire training process is presented, including the preparation and monitoring of the training.

Setup

The training workflow was carried out using the command-line interface of the MACE framework in a Linux environment under Windows Subsystem for Linux (WSL), accessed via Visual Studio Code (VS Code). To ensure compatibility and avoid conflicts between the different dependencies, a virtual environment was created.

Training

The following code provides an example on how to execute the training process in the MACE command line interface.

```
mace_run_train \
--name="MACE_model" \
--train_file="output.xyz" \
--valid_fraction=0.10 \
--config_type_weights='{"Default":1.0}' \
--E0s="{74:-4.495, 34:-8.989}" \
--model="MACE" \
--hidden_irreps='128x0e + 128x1o' \
--r_max=5.0 \
--batch_size=20 \
--max_num_epochs=1000 \
```

```
--stage_two \
--start_stage_two=800 \
--ema \
--ema_decay=0.99 \
--amsgrad \
--restart_latest \
--device=cuda \
--plot_frequency=5 \
--eval_interval=5 \
--compute_forces=True \
--compute_stress=True \
--energy_key=energy \
--forces_key=forces \
--stress_key=stress \
--energy_weight=1.0 \
--forces_weight=1.0 \
--stress_weight=1.0 \
--wandb \
--wandb_project="name_of_project" \
--wandb_entity="max_mustermann_tu_wien" \
--wandb_name="training_run_01"
```

The following list provides an explanation of the most relevant terms:

- **train_file**

Path to the training file (.xyz-file). If stored in another place than the regular /mace folder, the path needs to be included.

- **valid_fraction**

Fraction of the dataset that is used for validation.

- **E0s**

Reference energies of the single atoms.

- **max_num_epochs**

Maximum number of training epochs.

- **stage_two**

Starts a second, "fine-tuning" training.

- **start_stage_two**

Epoch number after which the second training begins.

- **device**

Enables training on the GPU using devide=cuda.

3. METHODS AND IMPLEMENTATION

- **wandb**

Integration with the W&B tool to monitor the progress.

Technical Aspects

The training was carried out on an NVIDIA GPU with CUDA support to enable accelerated tensor operations.

Monitoring

The training progress was monitored using the W&B interface, which allows real-time tracking of relevant metrics such as number of epochs, total and validation loss, and RMSE of energy.

For an overview of the training metrics, see Chapter ??.

Trained Model

Once the training is completed, two files are generated. The `.model` file contains all weights and parameters that were obtained during the training, whereas the `.json` file contains all metadata ensuring reproducibility. Combining these two files with ASE enables further applications.

3.5 Model Evaluation and Validation

The performance of the MACE model was evaluated by its ability to reproduce DFT reference data and physical trends within the system studied for both pristine and defective configurations.

4

CHAPTER

Results and Discussion

This chapter analyzes the phonon properties of monolayer WSe₂ using the MACE model. Furthermore, it discusses how structural defects influence the vibrational behavior of the systems and examines the influence of different supercell sizes.

All phonon-related calculations were performed using **Phonopy** and **ASE**, based on the results of the trained **MACE** force field. The visualizations were produced with **Matplotlib**.

4.1 Phonon Properties of Pristine WSe_2

4.1.1 Phonon Band Structure and Phonon Density of States of Pristine WSe_2

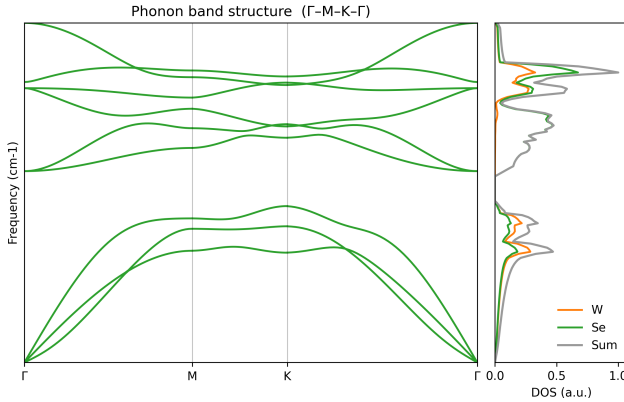


Figure 4.1: Phonon band structure and total phonon density of states of a pristine monolayer WSe_2 supercell (6x6). The left panel shows the phonon dispersion relation, while the right panel displays the total phonon DOS obtained by summing all atomic contributions.

The phonon band structure of pristine monolayer WSe_2 (Figure 4.1) shows the expected characteristic features. The primitive cell consists of three atoms, one W atom and two Se atoms, which create nine different phonon branches, as explained in Chapter 2. These nine phonon branches consist of three acoustic modes and six optical modes. The acoustic branches start at the Γ -point with a frequency of zero while the optical branches appear to have nonzero frequencies, which are visibly separated from the acoustic ones. The different masses of W and Se atoms lead to a divided vibrational spectrum into W- and Se dominated regions: the low-frequency modes are primarily dominated by the heavier W atom, while the lighter Se atoms contribute mainly to the higher-frequency modes.

4.1.2 Projected Phonon Density of States

The phonon DOS of pristine monolayer WSe_2 (Figure ??) quantify the number of vibrational modes per frequency interval and therefore reveal the separation between the acoustic and optical contributions.

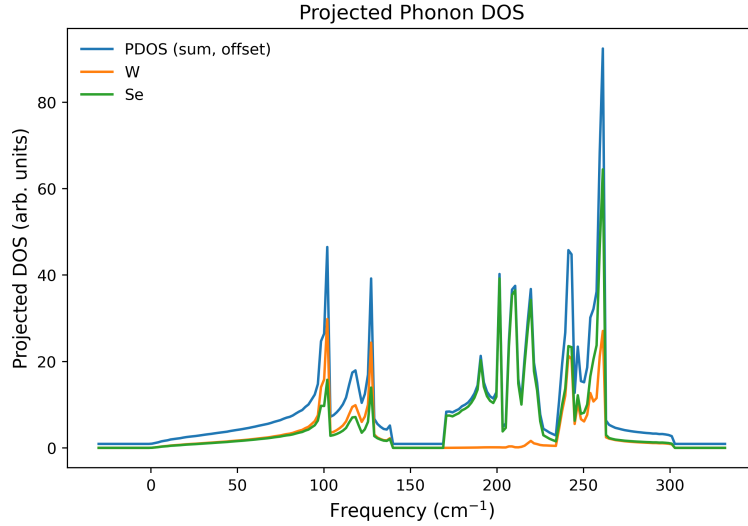


Figure 4.2: Projected phonon DOS of W and Se atoms in a pristine 6x6 WSe_2 supercell. The vibrational modes are projected on atomic displacements, exhibiting the contributions of the different elements.

Figure 4.2 shows the PDOS for the different atoms and highlights the contribution of W and Se to the vibrational spectrum.

4.2 Phonon Properties of Defective WSe_2

To analyze the phonon properties of defective WSe_2 and compare them to the pristine system, a Se vacancy is introduced. This vacancy breaks the translational symmetry, leading to the appearance of localized vibrational modes and shifts in the phonon density of states.

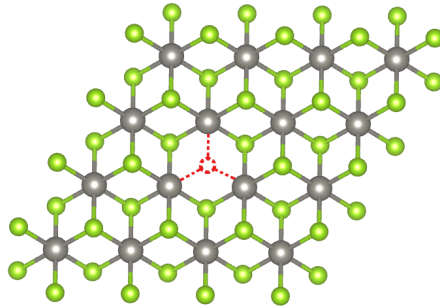


Figure 4.3: Illustration of a selenium vacancy in monolayer WSe_2 .

4. RESULTS AND DISCUSSION

4.2.1 Phonon Band Structure, DOS and PDOS of Defective WSe₂

In the following, the impact of a single selenium vacancy on phonon properties in monolayer WSe₂ is demonstrated.

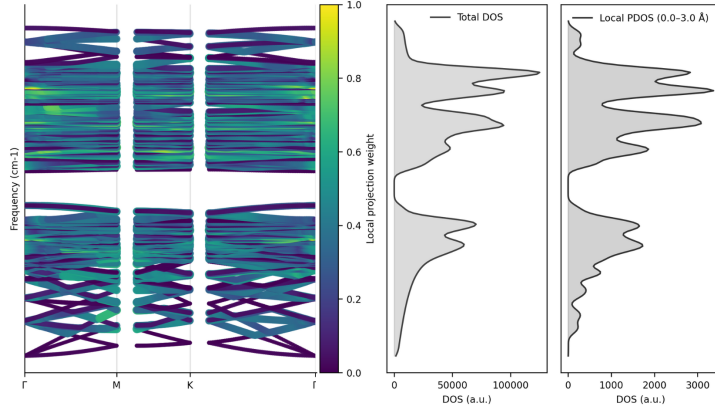


Figure 4.4: Phonon band structure, total DOS and local PDOS of a 6x6 WSe₂ supercell containing a Se vacancy.

The phonon band structure and the associated DOS of the defective supercell confirm a characteristic pattern of defect-induced vibrational behavior. It shows additional flat bands at mid to high frequencies, indicating localized vibrational modes around the Se vacancy.

The color scale demonstrates the local projection weight. It shows that those modes are limited near the vacancy.

The total DOS resembles the overall spectrum of pristine WSe₂, indicating that the impact of the vacancy is localized.

In comparison, the local PDOS show distinct peaks at optical frequencies, indicating defect-induced localized vibrational modes.

4.3 Comparative Analysis: Pristine vs Defect

This section provides a comparison of the phonon properties of pristine and defective 12x12 WSe₂ supercells, demonstrating the effect of a Se vacancy on the vibrational spectrum as well as dispersion characteristics.

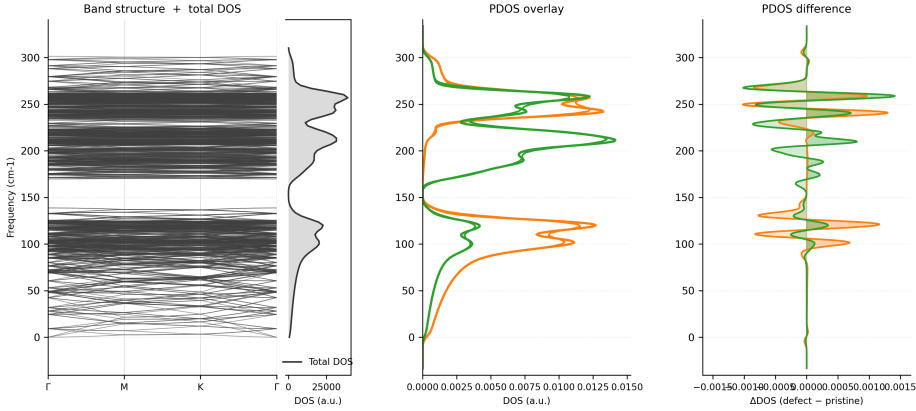


Figure 4.5: Combined phonon band structure, PDOS overlay and PDOS difference: pristine vs defective 12x12 supercell.

The comparison between pristine and defective configurations exhibits a difference in phonon spectra. The presence of the Se vacancy modifies the phonon band structure, visible as flat bands at certain frequencies and as peaks in the PDOS difference, indicating the emergence of localized vibrational modes.

4.4 Localized Vibrational Modes around the Vacany

In order to analyze the radial distribution of vibrational states in defective WSe₂, the phonon DOS was resolved as a function of distance from the Se vacancy for pristine and defective configurations. Splitting the surrounding atoms into three radial shells allows a distinction of local vibrational near the defect.

4. RESULTS AND DISCUSSION

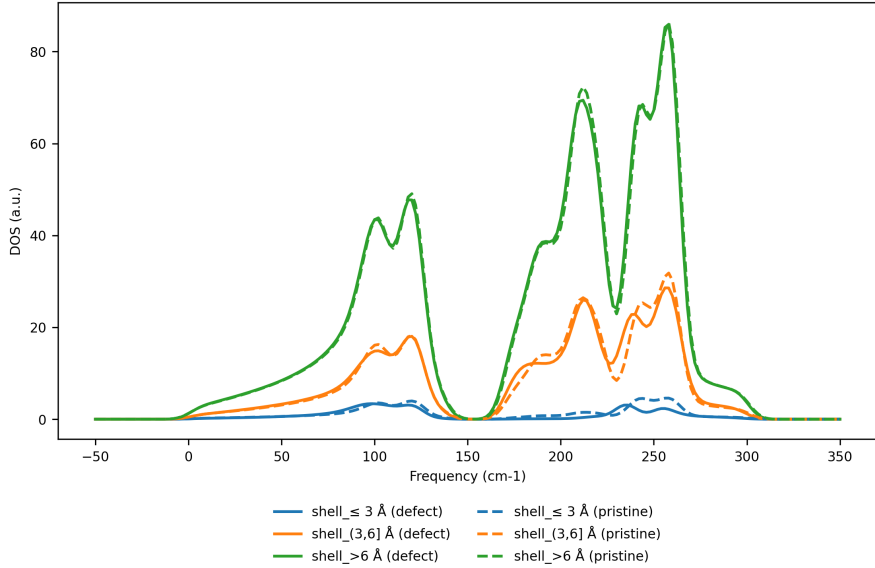


Figure 4.6: Radial phonon DOS of both, pristine and defective 6x6 WSe₂ supercells for different distances from the Se vacancy.

Figure 4.6 compares the radial dependence of the phonon DOS between the pristine and defective system. It shows that both systems, pristine and defective, exhibit similar phonon density of states, confirming that the influence of the Se vacancy is localized and the difference between the two systems decreases with increasing distance.

4.5 Physical Interpretation and Limitations

As the MACE model successfully reproduces energies and forces with near-DFT accuracy, its results still rely on the quality and variety of reference data. It learns the PES directly from the atomic configurations provided in the DFT data, transmitting any bias or limitation to the resulting MLFF. In general, the predictions align very well with the reference values, indicating that the model is capable of correctly understanding the underlying physical interactions.

However, despite all their advantages, MLFFs are still approximations that cannot provide direct access to certain electronic quantities such as band gaps or exciton binding energies. Further, the model is only defined up to a certain cutoff radius, neglecting long-range van der Waals interactions. This may be acceptable for short-range applications as in WSe₂, but becomes problematic when used otherwise.

There are still open questions on which MLFFs provide only limited insight, especially the detailed mechanism behind single-photon emission. Future combinations with electronic-structure models may provide a deeper insight into this.

4.6 Summary of Results

In this chapter, significant phonon properties of pristine and defective WSe₂ were analyzed using MLFFs of the MACE model. The results show an accurate reproduction of the phonon dispersion relation of pristine WSe₂, the contribution of both W and Se atoms, and the impact of the supercell size on the convergence of the vibrational spectrum.

Inducing a single Se vacancy causes changes in the phonon spectrum: additional flat modes in higher-frequency regions, which do not appear in the pristine counterpart. As shown in Section 4.4, these modes are localized to atoms around the defect, mainly to the nearest W atoms.

The comparative analysis of different supercell sizes in Section 4.3 provides proof that these features are caused by the vacancy itself, not by finite-size effects.

This suggests that the MACE model is capable of capturing defect-induced changes in vibrational properties and therefore provides a solid basis for further research.

CHAPTER 5

Conclusion and Outlook

This final chapter summarizes the key results of this thesis and discusses potential future applications, suggesting an extension of the presented approach for follow-up studies.

5.1 Conclusion

In this thesis, the inherent machine-learned force fields of the equivariant graph neural network MACE were trained with the primary goal of investigating the effect of a single selenium vacancy on the phonon spectrum and analyzing defect-related vibrational features.

The trained MACE model can successfully predict energies and forces with near DFT accuracy and help to precisely reproduce the phonon dispersion relation, density of states and projected density of states. This shows the reliability of the model and a certain stability of the underlying workflow.

Furthermore, the analysis of defect-induced structures shows the appearance of localized vibrational modes restricted to the immediate surroundings of the vacancy, which are visible as peaks in PDOS plots as well as flat bands in the dispersion. Since these modes are consistent across different sizes of supercells, finite-size effects can be excluded.

This shows the capability of Machine Learning Force Fields to capture local defects in complex atomic structures, providing a solid foundation for linking local defects in the crystal lattice to the formation of defect-bound excitons, which might represent the microscopic origin of single-photon emission.

5.2 Outlook

This thesis may form the foundation for several directions in future work. First, extending the dataset with additional types of defects – such as substitutional impurities, multiple

5. CONCLUSION AND OUTLOOK

vacancies, or strained configurations – allows a more in-depth analysis of defective phonon properties. Furthermore, including larger supercells could even improve the generalization capability of the model.

Secondly, by combining the predicted phonon properties with calculations of electronic band structure or excitons, the correlation between local lattice vibrations and defect-related electronic states could be investigated. This provides a promising way for achieving a better understanding of the formation of single-photon emitters in two-dimensional semiconductors.

Overview of Generative AI Tools Used

ChatGPT (OpenAI, GPT-5, 2025)

ChatGPT was used as a generative AI tool to support the writing of this thesis. Specifically, it assisted with:

- *language editing and translation (German–English, academic phrasing),*
- *technical formatting (LaTeX integration, figure generation, code snippets),*
- *conceptual structuring (summaries, draft formulations, organizational suggestions).*

All scientific content was critically reviewed, validated, and cross-checked with standard literature.

List of Figures

2.1	Schematic illustration of a monoatomic linear chain with a longitudinal displacement of a single atom [4]	4
2.2	Dispersion of Diatomic Chain: Acoustic and Optical Modes, calculated using ASE.	6
2.3	Schematic illustration of single-photon emitter in WSe ₂ , taken from [3].	7
2.4	Schematic illustration of a single GNN layer, taken from [10]. Every node, edge and global feature vector are updated by separate MLPs, while the graph connectivity stays fixed	9
3.1	Pipeline of the project: from DFT data generation to training, evaluation, and application of the trained MACE model.	13
3.2	Comparison of active learning (a) and Bayesian optimization (b), taken from [13].	16
4.1	Phonon band structure and total phonon density of states of a pristine monolayer WSe ₂ supercell (6x6). The left panel shows the phonon dispersion relation, while the right panel displays the total phonon DOS obtained by summing all atomic contributions.	22
4.2	Projected phonon DOS of W and Se atoms in a pristine 6x6 WSe ₂ supercell. The vibrational modes are projected on atomic displacements, exhibiting the contributions of the different elements.	23
4.3	Illustration of a selenium vacancy in monolayer WSe ₂	23
4.4	Phonon band structure, total DOS and local PDOS of a 6x6 WSe ₂ supercell containing a Se vacancy.	24
4.5	Combined phonon band structure, PDOS overlay and PDOS difference: pristine vs defective 12x12 supercell.	25
4.6	Radial phonon DOS of both, pristine and defective 6x6 WSe ₂ supercells for different distances from the Se vacancy.	26

Acronyms

ASE Atomic Simulation Environment. 17, 18, 20, 21

BZ Brillouin Zone. 7

DFT Density Functional Theory. 1, 8, 14–16, 20, 26, 29

DOS Density of States. 5, 6, 14, 18, 22–26, 33

GNN Graph Neural Network. 1, 3, 9, 33

MLFF Machine Learning Force Field. 8, 13–15, 17, 26, 27

MPNN Message Passing Neural Network. 9, 10

PDOS Projected Density of States. 18, 23–25, 29, 33

PES potential energy surface. 15, 17, 26

Se selenium. 7, 22–27, 33

SPE single-photon emitter. 1, 4

TMDC transition metal dichalcogenide. 3

TMDCs transition metal dichalcogenides. 1, 3

VASP Vienna Ab-initio Simulation Package. 14

VS Code Visual Studio Code. 18

W tungsten. 7, 22, 23, 27, 33

W&B Weights & Biases. 14, 20

WSe₂ tungsten diselenide. xiii, 1, 3, 4, 6, 7, 12–14, 16, 18, 21–27, 33

WSL Windows Subsystem for Linux. 18

Bibliography

- [1] Gui-Bin Liu, Di Xiao, Yugui Yao, Xiaodong Xu, and Wang Yao. Electronic structures and theoretical modelling of two-dimensional group-vib transition metal dichalcogenides. *Chemical Society Reviews*, 44(9):2643–2663, 2015.
- [2] Keliang et al. He. Tightly bound excitons in monolayer wse. *Physical Review Letters*, 113(2):026803, 2014.
- [3] Lukas Linhart, Matthias Paur, Valerie Smejkal, Joachim Burgdörfer, Thomas Mueller, and Florian Libisch. Localized intervalley defect excitons as single-photon emitters in wse₂. *Physical Review Letters*, 123(14):146401, 2019.
- [4] OpenAI. Chatgpt (version gpt-5). <https://chat.openai.com>, 2025. Large language model used for language editing, LaTeX support, and conceptual assistance.
- [5] Harald Ibach and Hans Lüth. *Festkörperphysik*. Springer-Verlag, Berlin Heidelberg, 7 edition, 2009.
- [6] Steven H. Simon. *The Oxford Solid State Basics*. Oxford University Press, Oxford, United Kingdom, 2013.
- [7] Oliver T. Unke, Stefan Chmiela, Hugo E. Saucedo, Michael Gastegger, Ivan Poltavsky, Kristof T. Schütt, Alexandre Tkatchenko, and Klaus-R Müller. Machine learning force fields. *Chemical Reviews*, 121(16):10142–10186, 2021. Preprint: arXiv:2010.07067 [physics.chem-ph].
- [8] Andriy Burkov. *The Hundred-Page Machine Learning Book*. Andriy Burkov, 2019. <http://thmlbook.com>.
- [9] Justin Gilmer, Samuel S Schoenholz, Patrick F Riley, Oriol Vinyals, and George E Dahl. Neural message passing for quantum chemistry. *arXiv preprint arXiv:1704.01212*, 2017.
- [10] Peter Battaglia, Michael Bronstein, and Petar Veličković. A gentle introduction to graph neural networks. *Distill*, 2021. <https://distill.pub/2021/gnn-intro>.

- [11] Ilyes Batatia, Dávid Péter Kovács, Gregor N. C. Simm, Christoph Ortner, and Gábor Csányi. MACE: Higher Order Equivariant Message Passing Neural Networks for Fast and Accurate Force Fields. *Advances in Neural Information Processing Systems*, 36, 2022. NeurIPS 2022.
- [12] Victor Garcia Satorras, Emiel Hoogeboom, and Max Welling. E(n) equivariant graph neural networks. *Proceedings of the 38th International Conference on Machine Learning*, pages 9323–9332, 2021.
- [13] Kevin P. Murphy. *Probabilistic Machine Learning: Advanced Topics*. MIT Press, 2023.